A Single-Wavelength Real-Time Material-Sensing Camera Based on ToF Measurements

Miguel Heredia Conde*, Otmar Loffeld*, Thomas Kerstein†, Bernd Buxbaum†

*Center for Sensor Systems (ZESS), University of Siegen, Paul-Bonatz-Straße 9-11, 57076 Siegen, Germany. E-mail: {heredia, loffeld}@zess.uni-siegen.de
†pmdtechnologies ag, Am Eichenhang 50, 57076 Siegen, Germany. E-mail: {T.Kerstein, B.Buxbaum}@pmdtec.com

Introduction

Different Materials Exhibit Different Scattering Phenomena

- Light reaching the surface of a material undergoes a set of scattering phenomena, such as surface scattering, surface-level inter-reflections, and subsurface scattering.
- The combined effect of all scattering phenomena on an incident light signal can be modeled by means of a time-domain *Material Impulse Response Function* (MIRF), denoted $h(t;\vec{p})$, with $\vec{p}$ a parameter vector.
- Different materials exhibit different MIRFs and, thus, MIRF-based material classification becomes possible.
- Time-of-Flight (ToF) sensors can be used to obtain Fourier samples of the MIRF over dense areas.

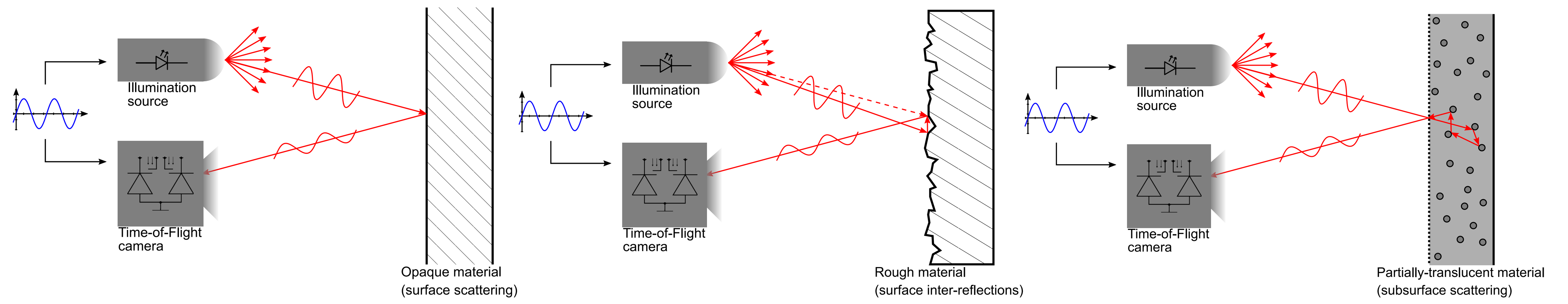

(a) Direct Surface Scattering (b) Surface Inter-Reflections (c) Subsurface Scattering

Figure 1: Schematics of the proposed material sensing concept showing different scattering phenomena undergone by incident light. (a): Direct surface scattering, as in a plain opaque surface. (b): Surface-level inter-reflections, as in rough or irregular surfaces. (c): Subsurface scattering, as in materials that are not perfectly opaque (e. g., colloidal suspensions).

PMD ToF Technology

- The Photonic Mixer Device (PMD) is a core technology for AMCW-ToF depth imaging.
- (Quasi-)sinusoidally-modulated NIR (ours: 940 nm) illumination. Modulation frequencies: 20-160 MHz.
- A binary reference signal drives the separation of photogenerated charges into two integration wells.

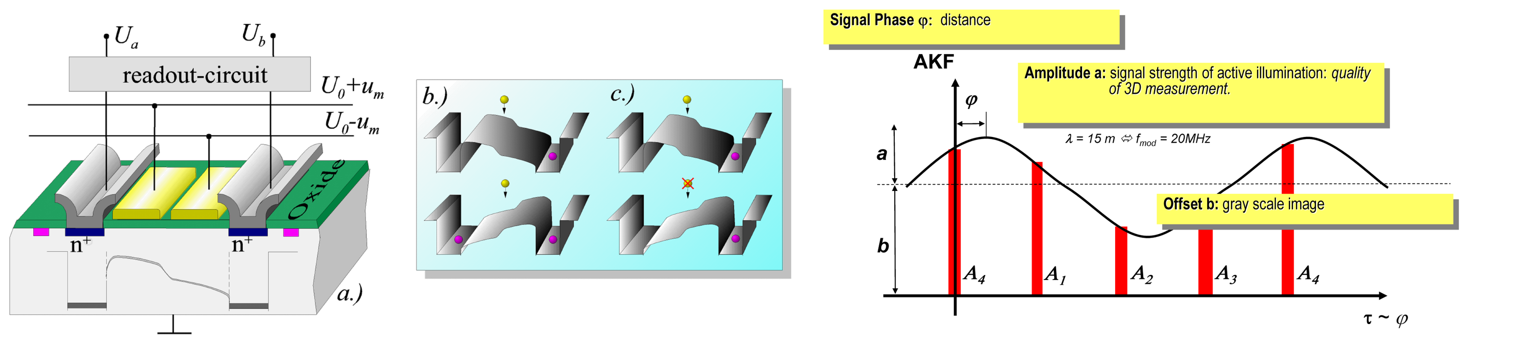

Figure 2: a.) Schematic of a PMD pixel and controlled integration of: b.) DC light and c.) modulated light.

- Low-pass filtering effects lead to a quasi-sinusoidal cross-correlation function.The phase shift (thus the depth) and the amplitude can be retrieved from few (e. g., $Q = 4$) samples:

$$\phi = \tan^{-1}\left(\frac{A_1 - A_3}{A_2 - A_4}\right), \quad d = \frac{c}{4\pi f_{\mathrm{mod}}}\phi, \quad a = \frac{\sqrt{(A_1 - A_3)^2 + (A_2 - A_4)^2}}{2} \tag{1}$$

MIRF Fourier Sampling with PMD Sensors

- Let a material be modeled by the MIRF $h(t;\vec{p}) \in \mathcal{B}_\Omega$, such that $\widehat{h}(\omega) = 0, |\omega| > \Omega$, where Ω is the bandwidth of $h(t;\vec{p})$ and $\vec{p}$ is a set of parameters that are both material an scene-dependent.
- For any desired frequency ω_k, such that $|\omega_k| \leq \Omega$ and $1 \leq k \leq K$, the CW-ToF camera uses a periodic illumination modulation function $p_k(t)$ with period $\Delta_k = 2\pi/\omega_k$ to probe the MIRF.
- After reaching the material surface, $p_k(t)$ is affected by surface-level and subsurface scattering, modeled by $h(t;\vec{p})$, and the signal reflected to the camera is $r_k(t) = (p_k * h_k)(t)$ where $*$ denotes convolution.
- In the PMD pixels we use, the same signal is used both for modulation and demodulation, up to a shift τ. Thus, the demodulation signal is $\psi_k(t) = p_k(t+\tau)$. Using different delays τ_q, $q \in \mathbb{N}$, a set of raw measurements at frequency ω_k can be obtained, which follow the model:

$$m_k[q] = (\overline{r}_k * p_k)(\tau_q) = (r_k \otimes p_k)(\tau_q) \tag{2}$$

where $\otimes$ denotes cross-correlation operation and $\overline{r}_{\mathbf{r}}(t) = r_{\mathbf{r}}(-t)$.

- From a sufficiently large number of measurements per frequency, Q, using $\tau_q = 2\pi q/(Q\omega)$ for $q = 1,\dots,Q$, an estimate of $\widehat{h}[k]$ can be obtained. In PMD ToF cameras $Q = 4$ and the method for obtaining the **phase** and **amplitude** of $\widehat{h}[k]$ is known as the *four phases algorithm*, outlined in (1).

Methodology

Hardware and Software Highlights

- **Hardware:** new-generation PMD Selene module
  - Extremely-low size: 11.5 mm × 7.0 mm × 4.2 mm
  - Fourier sampling demonstrated for real-time multipath estimation in [1].
- Depth- and reflectivity-independent features based on the MIRF Fourier samples, $\vec{f}_{u,v} \in \mathbb{C}^N$, where $N = K - 1$, are computed pixelwise, similar to [2, 3]:

$$\left|\vec{f}_{u,v}\right| = \left[\frac{\left|\widehat{h}[k']\right|}{\left|\widehat{h}[k_{\mathrm{ref}}]\right|}\right]_{k' \neq k_{\mathrm{ref}}} \qquad \angle\vec{f}_{u,v} = \left[\angle\widehat{h}[k'] - \left(\frac{k'}{k_{\mathrm{ref}}}\right)\angle\widehat{h}[k_{\mathrm{ref}}]\right]_{k' \neq k_{\mathrm{ref}}} \tag{3}$$

where k_{ref} denotes the index of the reference frequency, e. g., $k_{\mathrm{ref}} = 1$, and $1 \leq u \leq n_{\mathrm{rows}}$, $1 \leq v \leq n_{\mathrm{cols}}$, where $n_{\mathrm{rows}} \times n_{\mathrm{cols}}$ is the array size.

- Using the **MIRF-based** and **texture-independent** complex features $\vec{f}_{u,v}$ a classifier, such as a decision tree of a Support Vector Machine (SVM), is trained.

Importance of Harmonic Cancellation (HC)

- If both $p_k(t)$ and $\psi_k(t)$ are non-sinusoidal with overlapping harmonic content, then our estimate of $\widehat{h}[k]$ will suffer from harmonic distortion. → Two possibilities for ***a priori*** HC:
  - Apply a generic Q-phases algorithm, with a large enough number of samples Q. → Too slow for real time.
  - Bracketed exposure with ad-hoc phase shifts per bracket, as proposed in [4] → **Enabled by our own hardware**.

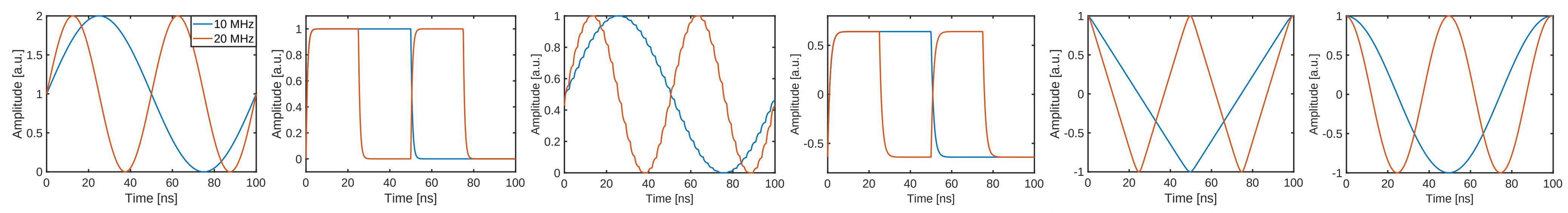

(a) Ideal Illumination (b) Realistic Illumination (c) Realistic Illumination with HC (d) Realistic PMD (A-B) Control Signal (e) Realistic PMD (A-B) Cross-Correlation (f) Realistic PMD (A-B) Cross-Correlation with HC

Figure 3: Relevant signals in our PMD-based ToF system from realistic simulations, with and without HC.

Experimental Results

Dense Per-pixel Material Classification

- Material classification carried out for each pixel, (u, v), using the feature vectors calculated in (3).
- A dataset consisting of 5 different materials was acquired, gathering $K = 6$ frequencies per ToF frame, from 20 MHz to 120 MHz. A Gaussian kernel classification model was fitted using 30% of the data.

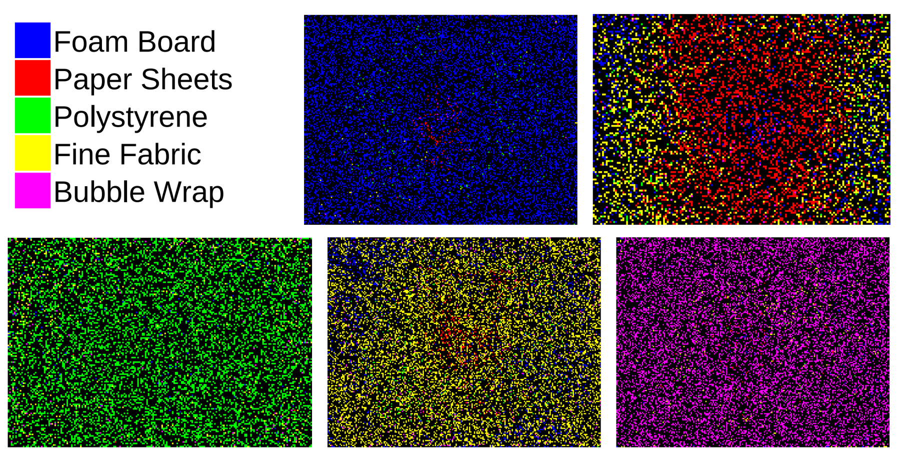

Figure 4: Per-pixel material classification. 30% of the pixels are randomly picked for training the classifier (masked in black). The remaining 70% are used for validation. Color code in the top-left. Accuracy: 78%.

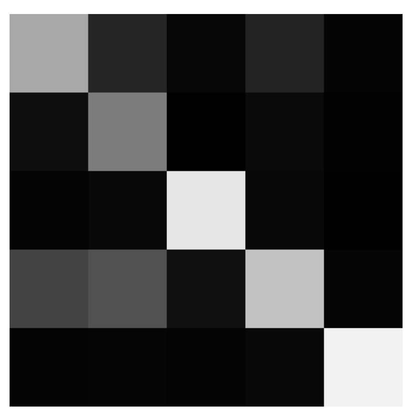

Figure 5: Confusion matrix corresponding to the results in Fig. 5. Ground truth per columns and prediction per rows. Rows and columns according to Fig. 5-top-left. White: 100% accuracy.

Superpixel-based Material Classification

- Performing a classification query for all pixels in the array is time consuming for large array sizes. Furthermore, pixels belonging to the same material are typically grouped together.
- Boundaries in the 2D image domain can be found where the MIRF, thus $\vec{f}_{u,v}$, changes abruptly. A single or very few classification queries per superpixel suffice for robustly classifying the region's material.

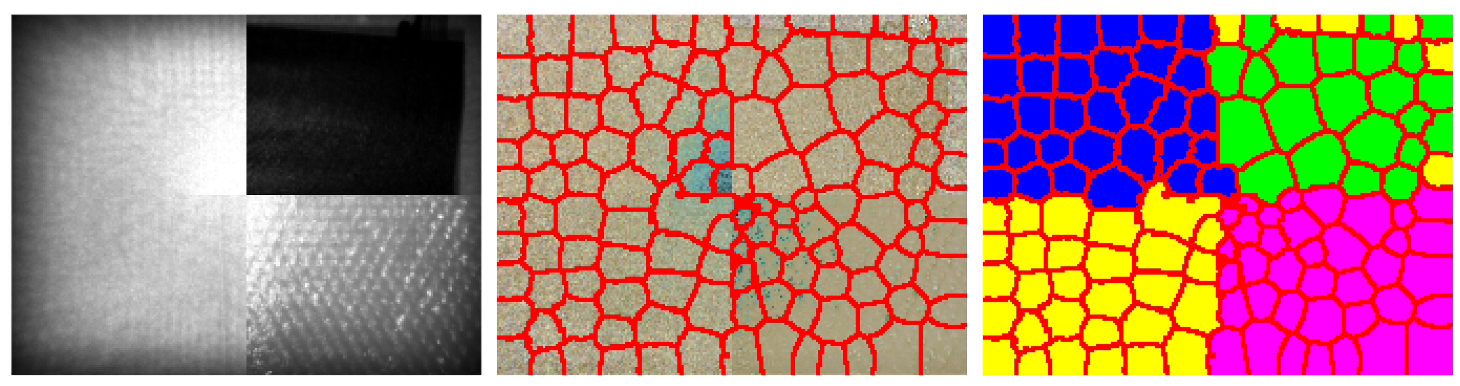

(a) NIR DC Image (b) Superpixel Boundaries (c) Superpixel-based Classification Result

Figure 6: Superpixel-based classification. The classifier is trained as before, using 30% of randomly-selected pixels. (a): NIR DC image of a composition of four materials. Color code in Fig. 5-top-left. (b): Superpixel boundaries detected using $\vec{f}_{u,v}$. (c): Classification result from 10 classification queries per superpixel. At superpixel scale accuracy is close to 100%.

References

[1] M. Heredia Conde, A. Bhandari, T. Kerstein, B. Buxbaum, and O. Loffeld, "Live Demonstration: Multiple-path depth imaging with time-of-flight sensors," in *2019 IEEE SENSORS*, Oct. 2019.

[2] S. Su, F. Heide, R. Swanson, J. Klein, C. Callenberg, M. Hullin, and W. Heidrich, "Material classification using raw time-of-flight measurements," in *2016 IEEE Conference on Computer Vision and Pattern Recognition (CVPR)*, June 2016, pp. 3503–3511.

[3] K. Tanaka, Y. Mukaigawa, T. Funatomi, H. Kubo, Y. Matsushita, and Y. Yagi, "Material classification from time-of-flight distortions," *IEEE Transactions on Pattern Analysis and Machine Intelligence*, vol. 41, no. 12, pp. 2906–2918, Dec 2019.

[4] A. D. Payne, A. A. Dorrington, M. J. Cree, and D. A. Carnegie, "Improved linearity using harmonic error rejection in a full-field range imaging system," in *Proc. SPIE*, vol. 6805, 2008, pp. 6805 – 6805 – 11.